Journal of Solid State Chemistry 184 (2011) 1421–1427

Contents lists available at ScienceDirect

Journal of Solid State Chemistry

journal homepage: www.elsevier.com/locate/jssc

Green synthesis of graphene nanosheets/ZnO composites and electrochemical properties

Jun Wang [a,b,*], Zan Gao [a,b], Zhanshuang Li [a], Bin Wang [a], Yanxia Yan [a], Qi Liu [a], Tom Mann [b], Milin Zhang [a,b], Zhaohua Jiang [c]

[a] College of Material Science and Chemical Engineering, Harbin Engineering University, Harbin 150001, PR China
[b] The Key Laboratory of Superlight Materials and Surface Technology, Ministry of Education, Harbin 150001, PR China
[c] College of Chemical Engineering, Harbin Institute of Technology, Harbin 150001, PR China

ARTICLE INFO

Article history:
Received 19 November 2010
Received in revised form
27 January 2011
Accepted 3 March 2011
Available online 12 April 2011

Keywords:
Graphene nanosheet
ZnO
Composite electrode
Supercapacitor

ABSTRACT

A green and facile approach was demonstrated to prepare graphene nanosheets/ZnO (GNS/ZnO) composites for supercapacitor materials. Glucose, as a reducing agent, and exfoliated graphite oxide (GO), as precursor, were used to synthesize GNS, then ZnO directly grew onto conducting graphene nanosheets as electrode materials. The small ZnO particles successfully anchored onto graphene sheets as spacers to keep the neighboring sheets separate. The electrochemical performances of these electrodes were analyzed by cyclic voltammetry, electrochemical impedance spectrometry and chronopotentiometry. Results showed that the GNS/ZnO composites displayed superior capacitive performance with large capacitance (62.2 F/g), excellent cyclic performance, and maximum power density (8.1 kW/kg) as compared with pure graphene electrodes. Our investigation highlight the importance of anchoring of small ZnO particles on graphene sheets for maximum utilization of electrochemically active ZnO and graphene for energy storage application in supercapacitors.

1. Introduction

The increasing demand for energy and growing concerns about air pollution, global warming and the development of renewable energy production, hybrid electric vehicles with low CO_2 emission have stimulated intense research on energy storage and conversion from alternative energy sources [1]. Supercapacitors (SCs), also called electrochemical supercapacitors (ESCs) or ultracapacitors, are considered as promising candidates for energy storage due to high power performance, long cycle life, and low maintenance cost [2,3]. Compared with secondary batteries, supercapacitors can provide high power in short-term pulses, and can be used as peak-power sources in hybrid electric vehicles, memory backup devices, or back-up supplies to protect against power disruption [4].

Supercapacitors can be categorized into two main types based on their charge-storage mechanisms: (i) electrical double-layer capacitors (EDLCs), where the electrical charge is stored at the interface between the electrode and the electrolyte; (ii) redox electrochemical capacitors, where capacitance arises from reversible Faradaic reactions taking place at the electrode/electrolyte interface [2]. To date, carbon materials [5], transition metal oxides [6–11] and conducting polymers [12–15] have been identified as most promising materials for SCs. However, each material has its unique advantage and disadvantage for SCs application. For example, carbon material has high power density and long life cycle, but the small double layer capacitance limits its application. Transition metal oxides, hydroxides and conducting polymers have relative higher capacitance and fast redox kinetics, while the relative low mechanical stability and cycle life are major limitations for SCs. If different kinds of materials are integrated into the electrodes of SCs, their capacitive performance will be enhanced largely because most of the redox electrochemical (pseudo-capacitive) materials can contribute higher capacitance to the total capacitance, apart from the double-layer capacitance of carbon materials.

As a rising star in carbon family, two-dimensional graphene has attracted a great deal of attention due to its high surface area, electrical conductivity, high flexibility and mechanical strength since its discovery in 2004 [16,17]. Recently, one new perspective is to utilize ideal single-atom-thick GNS as a support to anchor functional nanomaterials to form new nanocomposites with potential application in catalysis, light energy conversion, fuel cells [18]. This perspective opens up new opportunities for designing next-generation electronic and energy conversion

* Corresponding author at: College of Material Science and Chemical Engineering, Harbin Engineering University, Harbin 150001, PR China. Fax: +86 451 8253 3026.
E-mail address: zhqw1888@sohu.com (J. Wang).

0022-4596/$ - see front matter © 2011 Elsevier Inc. All rights reserved.
doi:10.1016/j.jssc.2011.03.006

devices [19], since GNS has been shown excellent electrochemical behavior as electrodes of SCs [20–22]. Williams et al. [23] used a UV-assisted photocatalytic method to obtain photoactive graphene-semiconductor composites, opening up a new way to synthesize graphene-based nanocomposite materials. Wang et al. [7] made $Ni(OH)_2$ nanoplates grown on graphene, as advanced electrochemical pseudocapacitor materials, which exhibit a high specific capacitance and excellent cycling ability. Li et al. [24] fabricated SnO_2/graphene composite electrode materials by reducing graphene oxide with $SnCl_2$ and studied their application in SCs. GNS composites have shown its superior property as supercapacitor materials. However, research on the potential of graphene/metal oxide composite materials for supercapacitors has so far been limited.

ZnO, as a potential semiconductor with large band gap (3.37 eV), has received enormous scientific attention because of its promising applications [25–27]. And, ZnO is a well-known battery active material having high energy density of 650 A/g [28,29]. Recently, it has been used as a potential candidate for supercapacitor application. Selvakumar et al. [30] have fabricated nano ZnO/activated carbon composite electrodes for the first time which showed a specific capacitance of 84 F/g and good electrochemical reversibility. Lu et al. [31] successfully synthesized graphene/ZnO electrode materials by ultrasonic spray pyrolysis, which exhibited a specific capacitance of 61.7 F/g and maximum power density of 4.8 kw/kg. ZnO, therefore, is a promising electrode material for supercapacitors due to its electrochemical activity and eco-friendly nature.

In this work, we employed a green and facile approach to prepare GNS/ZnO composites. First, graphene nanosheets were synthesized via using glucose as a reducing agent [32], then ZnO was directly grown onto conducting graphene nanosheets to obtain GNS/ZnO composites. With this method the reductant and the oxidized product are environmentally friendly. And, the small ZnO particles homogeneously anchor onto graphene sheets, performing as spacers to keep neighboring sheets separate. The graphene sheets overlap with each other so that this factor not only affords a three-dimensional conducting network for fast electron transfer between the active materials and the charge collector, but also improves the contact between the electrode materials and the electrolyte. Electrochemical tests showed that these composites have a good reversible capacity, high coulombic efficiency, and excellent cyclic performance.

2. Experimental

2.1. Synthesis of GNS/ZnO composites

All the chemicals were of analytical grade and were used without further purification. The GNS/ZnO composites were synthesized via an in situ crystallization technique. GO was prepared from natural graphite by a modified Hummers method as described previously [33]. Exfoliation of GO was achieved by ultrasonication of the dispersion using an ultrasonic bath (KQ-500DB, 250 W). Compared with the traditional procedure using highly toxic hydrazine as reductant for chemical conversion of GO to GNS, we used glucose as a reducing agent to prepare GNS. Typically, 2 g glucose was added into 250 mL of homogeneous GO dispersion (0.5 mg/mL), followed by stirring for 30 min. Then 1 mL ammonia solution (25% w/w) was added to the resulting dispersion. After vigorously shaking for a few minutes, the mixture was stirred for 60 min at 95 °C. The resulting black dispersion was then filtered and washed with water for several times and the obtained GNS was redispersed in water for further use.

To synthesize GNS/ZnO composites, 250 mL of the as-obtained GNS suspension (0.5 mg/L) was transferred into a round bottom flask, then a certain amount of $Zn(NO_3)_2$ and NaOH solution (mole ratio was 1:10) was added into the above GNS suspension. The mixture was then heated to 95 °C with stirring for 5 h. We obtained GNS/ZnO composites with different mass ratios (GNS:ZnO was, respectively, 1:1, 1:2 and 1:3) by changing the amounts of GNS and ZnO. Finally, the composites were filtered, and washed several times with distilled water and alcohol, and dried at 80 °C for 12 h in a vacuum oven.

2.2. Characterization methods

The crystallographic structures of the materials were characterized by a powder X-ray diffraction system (XRD, TTR-III) equipped with Cu $K\alpha$ radiation ($\lambda = 0.15406$ nm). Raman measurements were performed with a Jobin Yvon HR800 micro-Raman spectrometer at 457.9 nm. The microstructure of the samples was investigated by an atomic force microscopy (AFM, Nanoscope IIIa), scanning electron microscopy (SEM, JEOL JSM-6480A microscope) and a transmission electron microscopy (TEM, PHILIPS CM 200 FEG, 160 kV).

2.3. Preparation of electrodes and electrochemical characterization

The working electrodes were fabricated by mixing the prepared powders with 15 wt% acetylene black and 5 wt% polytetrafluorene–ethylene (PTFE) binder. A small amount of ethanol was added to the mixture to produce a homogeneous paste. Then the resulting mixture was coated onto the nickel foam substrate (1 cm × 1 cm) with a spatula. The amount of composites onto the electrode including the electroactive material, conducting agent and binder was approximately 10 mg. The electrochemical properties of as-obtained products were investigated under a three-electrode cell configuration: The Ni foam coated with GNS/ZnO composites was used as working electrode, platinum foil (1 cm × 1 cm) and a saturated calomel electrode (SCE) as the counter and reference electrodes, respectively. The measurements were carried out in a 1 M KOH aqueous electrolyte at room temperature. Cyclic voltammograms (CV), galvanostatic charge/discharge and electrochemical impedance spectroscopy (EIS) were measured by a CHI 760b electrochemical work station. CV tests were done between −0.6 and 0.3 V (vs. SCE) at different scan rates of 5, 10, 20, and 40 mV s^{-1}. Galvanostatic charge/discharge curves were measured in the potential range of −0.6 to 0.2 V (vs. SCE) at different current densities of 5, 10, and 20 mA cm^{-2}, and EIS measurements were also carried out in the frequency range from 100 kHz to 0.05 Hz at open circuit potential with an ac perturbation of 5 mV.

3. Results and discussion

3.1. Formation mechanism and microstructure characterizations

Fig. 1 illustrates the fabrication process and formation mechanism for ZnO/GNS composites. As shown by previous studies, GO sheets have their basal planes covered mostly with epoxy and hydroxyl groups, while carbonyl and carboxyl groups are located at the edges [23]. These functional groups, acting as anchor sites, enable the subsequent in situ formation of nanostructures to attach to the surfaces and edges of GO sheets. However, these oxygen-containing functional groups impair the conductivity of GO sheets to such an extent that the GO sheets are not suitable for electrode materials. On the other hand, GNS have an excellent conductivity, with ideal single-atom thick

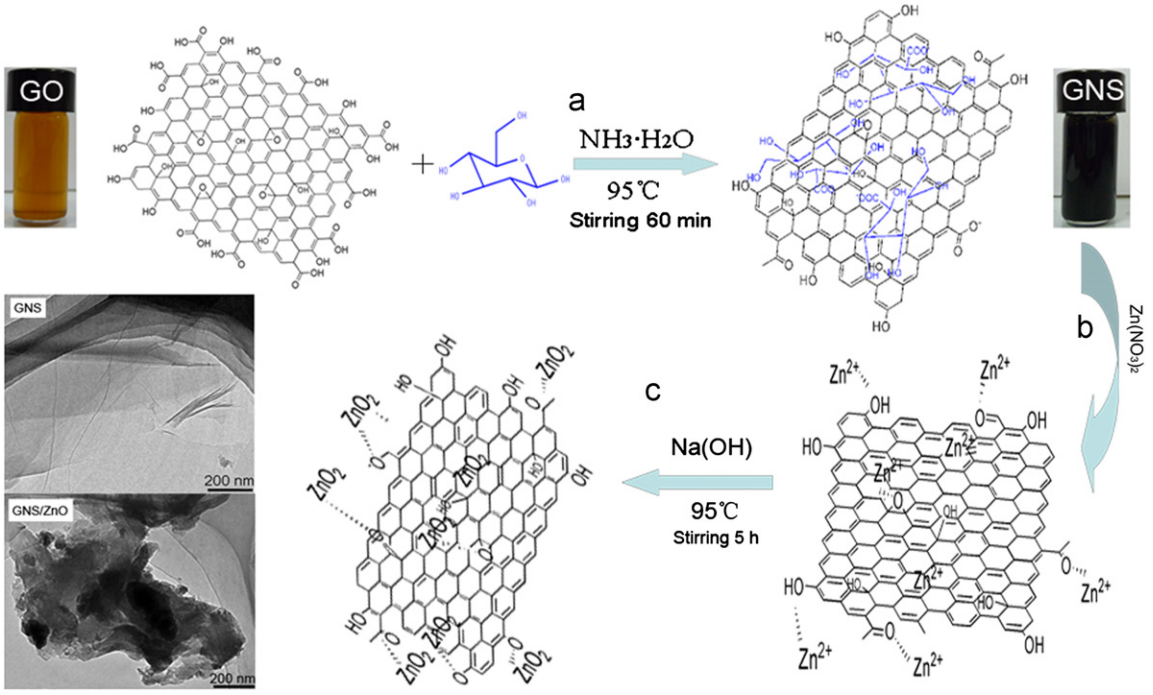

Fig. 1. Schematic representation of the fabrication process and formation mechanism for GNS/ZnO composite.

substrate for growth of functional nanomaterials to render them electrochemically active and electrically conductive. Step (a) shows the preparation of GNS based on glucose reducing GO, in which glucose as a reductant will remove most of the oxygen-containing groups. The oxidized products of glucose may also play an important role as a capping reagent in stabilizing as-prepared GNS.

After the reduction process, most oxygen-containing groups were removed, and the conductivity of GNS was recovered. But there are still some residual oxygen-containing groups on GNS [22,32]. When adding $Zn(NO)_3$ (step b) solution to GNS dispersion, Zn^{2+} ions will bind with the O atoms of the negatively charged residual oxygen-containing functional groups on GNS via an electrostatic force. With the addition of a solution of NaOH (step c) at a relatively higher temperature (approximately 95 °C), a large number of nuclei are formed in a short time from the reactions:

$$Zn^{2+} + 4OH^- \rightarrow Zn(OH)_4^{2-}$$

$$Zn(OH)_4^{2-} \rightarrow ZnO + H_2O + 2OH^-$$

The Zn atoms of the ZnO octahedron may form bonds with O atoms of the functional groups via a covalent coordination bond, acting as anchor sites for the crystals to grow. Finally, ZnO particles grow larger along the planes and the edges of graphene sheets to form GNS/ZnO composites.

Fig. 2 shows the XRD patterns of the natural graphite, GO, GNS and the as-prepared GNS/ZnO composites with different mass ratio. Compared with the natural graphite (Fig. 2, trace a), the feature diffraction peak of exfoliated GO at 10.8° (0 0 1) is observed with interlay space (d-spacing) of 0.8 nm (Fig. 2, trace b). This value is larger than the d-spacing (0.34 nm) of natural graphite ($2\theta = 26.5°$) as a result of the introduction of oxygenated functional groups. At the same time, the diffraction peak at $2\theta = 10.8°$ disappears for the XRD pattern of GNS, and the interlayer spacing of GO changes from 0.8 nm in GO to 0.37 nm in GNS, which is still a little larger than the d-spacing of natural graphite (0.34 nm). The small amount of oxygen-containing groups and hydrogen remaining may be the main reason for this difference,

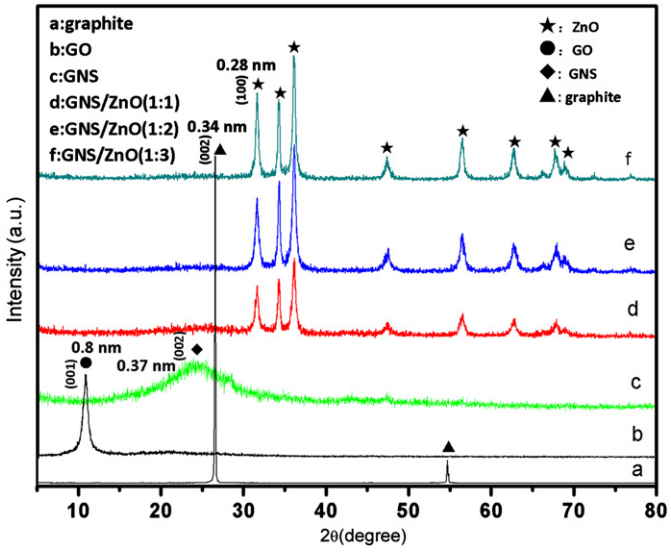

Fig. 2. Typical XRD patterns of natural graphite (a), GO (b), GNS (c) and the as-prepared GNS/ZnO composites (d–f).

indicating incomplete reduction of GO to graphene. These residual oxygenated functional groups are suggested as intercalation and adsorption of Zn^{2+} ions onto the GNS. The diffraction peaks of as-synthesized GNS/ZnO composites can be ascribed to the well-crystallized ZnO (JCPDS36-1451), where the (0 0 2) reflection peak of layered GNS has almost disappeared and the d-spacing of the (1 0 0) diffraction peak of ZnO is 0.28 nm.

Raman spectroscopy is a non-destructive and most widely used technique to characterize graphitic materials, in particular to determine ordered and disordered crystal structures of graphene [34]. The Raman spectrum of graphene is usually characterized by two main features, the G mode arising from the first order scattering of the E_{1g} phonon of sp^2 C atoms (usually observed at 1575 cm^{-1}) and the D mode arising from a breathing mode of

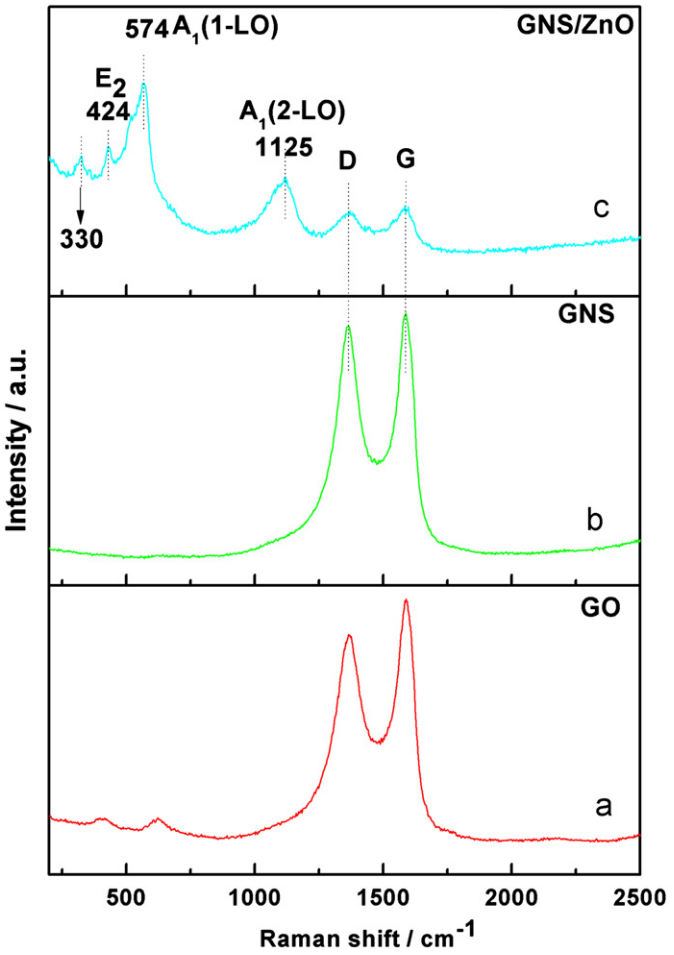

Fig. 3. Raman spectra of GO (a), GNS (b) and GNS/ZnO (c) composites.

point photons of A_{1g} symmetry (1350 cm^{-1}) [35]. The Raman spectra of GO, GNS and GNS/ZnO composites were shown in Fig. 3. A broad D band (1356 cm^{-1}) and a broad G band (1580 cm^{-1}) are observed in all samples. In general, the I_D/I_G intensity ratio is a measure of disorder degree and average size of the sp^2 domains in graphite materials [36]. Compared with GO (trace a), the increased I_D/I_G intensity ratio for GNS (trace b) was observed, indicates that a decrease in the size of the in-plane sp^2 domains [37], the removal of the oxygen functional groups in graphite oxide sheets and the restablishment of the conjugated graphene network (sp^2 carbon). For the Raman spectrum of GNS/ZnO composite (trace c), except the G band and D band, a typical Raman peak of ZnO particles at 424 cm^{-1} corresponding to the vibration mode of E_2 were observed. And, the additional low intensity peaks was observed at 330 cm^{-1}, which is known to be the vibration mode due to the multiple-phonon scattering processes of ZnO. Also, the peak at 574 and 1125 cm^{-1} are correspondent to the LO phonon of A_1 mode of ZnO [38,39].

Fig. 4 is a typical AFM image of exfoliated GO dispersion in water after their deposition on a freshly cleaved mica surface. The average thickness of as-prepared GO, measured from the height profile of the AFM image is about 1.1 nm, which corresponds to a single layer GO. Compared with the theoretical values of 0.78 nm for single layer graphene, the higher thickness of GO arise from oxygen-containing groups on the surfaces [40]. In this paper, utilizing this reduced graphene oxide as a two-dimensional carbon support to anchor ZnO nanoparticles provides a new way to develop supercapacitor electrode materials.

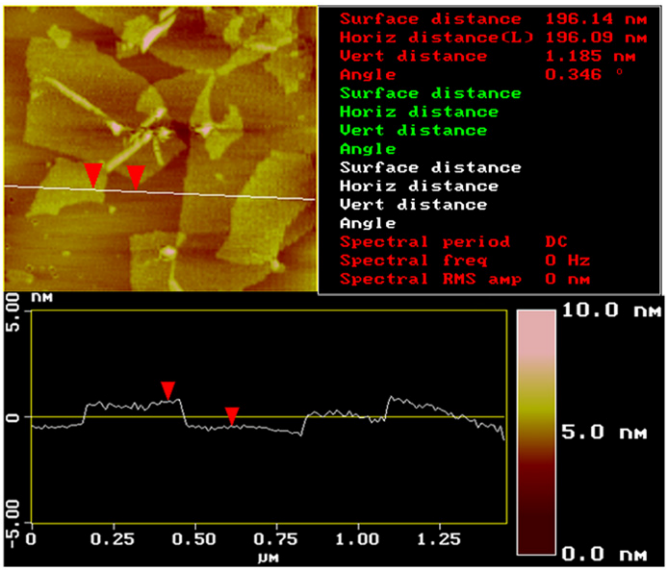

Fig. 4. AFM image of exfoliated GO sheets on mica surface with height profile.

Fig. 5 shows the morphology and dimension of the as-obtained products, in which most of the graphene nanosheets are curled and entangled together with a layered structure in the dry state (Fig. 5a), the inset TEM image shows that GNS has corrugations and scrollings on the edge of the graphene. Fig. 5 (b–d) shows the SEM images of GNS/ZnO composites with different mass ratio, from which we can see small ZnO particles are closely anchored onto the surface of graphene sheets due to the remaining oxygen-containing groups. With increasing mass ratio of ZnO, more ZnO particles deposite onto the edges and planes of GNS, enter the graphene sheets as spacers to prevent the restacking of graphene sheets, thus avoid/weak the loss of their high active surface area. And, graphene layers interact with each other because of the van der Waals interactions to form an open system, through which electrolyte ions easily access the surfaces of graphene, which facilitates the formation of electric double layers and improve the electrochemical utilization of ZnO. We also observed that, even after a long time of sonication during the preparation of the TEM specimen, the ZnO particles are still strongly anchored on the surface of graphene sheets with a high density, as shown in Fig. 5e, suggesting a strong interaction between ZnO particles and graphene sheets. Additionally, the lattice fringes with interplanar distances of approximately 0.28 nm shown in Fig. 5f, correspond to the (1 0 0) plane of the cubic ZnO structure, which is consistent with XRD results.

3.2. Electrochemical behavior

The performance of the graphene based electrodes is analyzed using CV, galvanostatic charge/discharge and EIS. The EIS data is analyzed using Nyquist plots. Each data point in Nyquist plot is at a different frequency. The galvanostatic charge/discharge was performed to calculate the specific capacitance of the electrode according the following equation:

$$C_{sp} = \frac{it}{\Delta v m} \quad (1)$$

where i, t, Δv and m are the constant current (A), discharge time (s), the total potential deviation (V) and the weight of active materials (g), respectively.

Fig. 6 shows CV curves of GNS and GNS/ZnO composite electrodes under the potential from −0.6 to 0.3 V. The shapes of

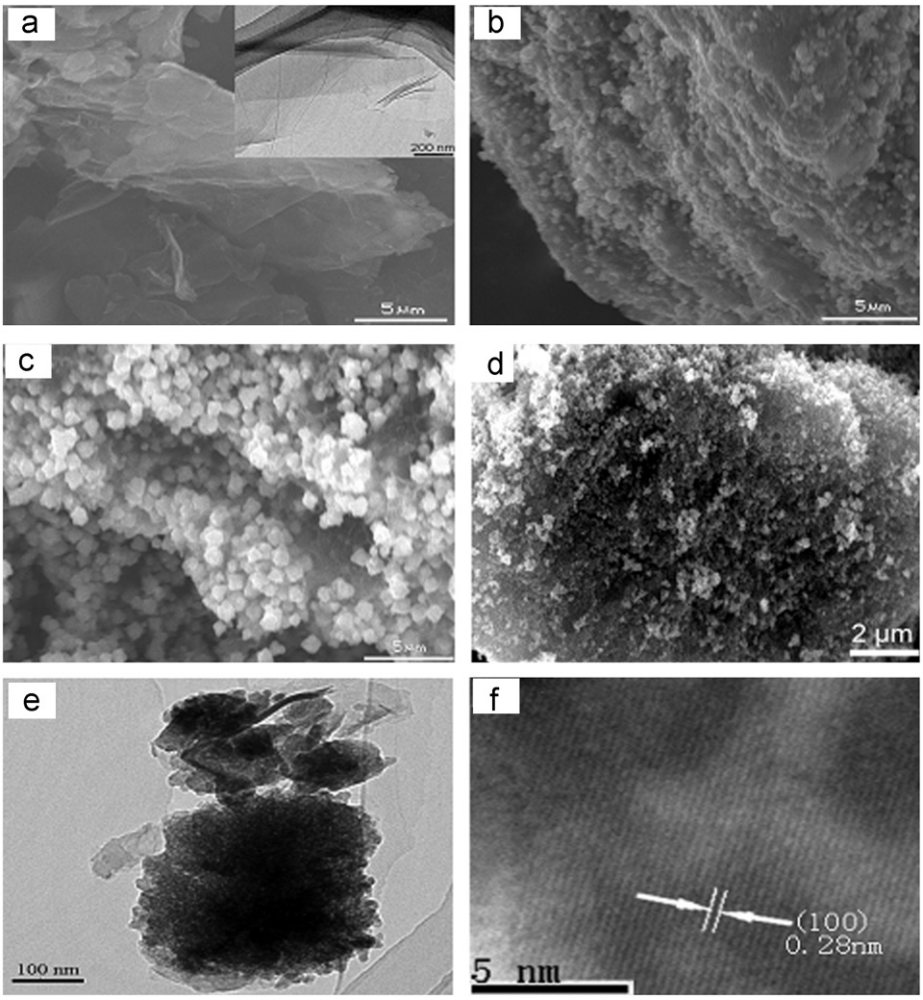

Fig. 5. (a) SEM images of pure GNS (inset exhibits the corresponding TEM images), (b–d) SEM images of GNS/ZnO (1:1), GNS/ZnO (1:2), GNS/ZnO (1:3) composites, (e and f) TEM and HRTEM images of GNS/ZnO composites.

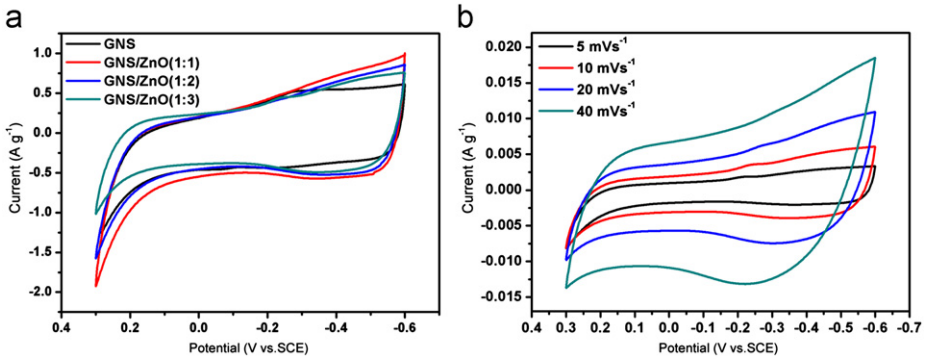

Fig. 6. CV curves of GNS and GNS/ZnO composites with different mass ratio at a scan rate of 10 mV s^{-1} in 1 M KOH solution (a), CV curves of GNS/ZnO (1:1) composites at different scan rates of 5, 10, 20, and 40 mV s^{-1} in 1 M KOH solution.

CV loops in our experiment are quasi-rectangular along the current–potential axis without obvious redox peaks, indicating that all samples have a good capacitive behavior in SCs [41]. A larger current density response is observed for the GNS/ZnO (1:1) composite electrode implying a higher specific capacitance than that of pure GNS and other GNS/ZnO composites at the same scan rate (Fig. 6a), resulting from the high accessibility of electrolyte ions. AC Impedance spectroscopy also supports this observation. For GNS/ZnO (1:1) sample (Fig. 6b), no obvious distortion is observed in the CV curves as the potential scan rates are increased. The observed rectangular type plots are indicative of good capacitive behavior. Furthermore, the obvious increase of current with scan rates means a desirable rate capability for GNS/ZnO composite electrode.

The EIS analysis is one of the principal methods to examine the fundamental behavior of electrode materials for SCs [2]. For further understanding, impedance of the pure GNS and the GNS/ZnO composites were measured in the frequency range of 100–0.05 kHz at open circuit potential with an ac perturbation of 5 mV (Fig. 7). Each impedance spectrum has a semicircle arc and

a straight line. The high-frequency arc corresponds to the charge transfer limiting process and is ascribed to the double-layer capacitance (C_{dl}) in parallel with the charge transfer resistance (R_{ct}) at the contact interface between electrode and electrolyte solution. R_{ct} can be directly measured as the semicircle arc diameter [22]. The values of R_{ct} for GNS/ZnO composite electrodes are: (GNS/ZnO (1:1) 2.87 Ω; GNS/ZnO (1:2) 3.95 Ω; and GNS/ZnO (1:3) 5.59 Ω, respectively), i.e. the values increase as the mass ratio of ZnO increases. All values are larger, however, than that of pure GNS (1.36 Ω), indicating that the incorporation of GNS improves the charge transfer performance of GNS/ZnO electrode.

The equivalent series resistance (ESR) can be obtained from the X-intercept of the Nyquist plot, which determines the rate that the ESCs can be charged/discharged (power capability). The ESR, as shown in Fig. 7, is 1.51 Ω for pure GNS, 2.89 Ω for GNS/ZnO (1:1), 4.12 Ω for GNS/ZnO (1:2) and 5.84 Ω for GNS/ZnO (1:3), respectively. For GNS/ZnO composites the ESR of GNS/ZnO (1:1) is smaller than other composites, which may be attributed to the structure facilitating the efficient access of electrolyte ions to the surface of ZnO and graphene. At low frequencies, the impedance plot should theoretically be a vertical line, which is parallel to the imaginary axis. In fact, the low frequency straight line always departs from that expected with a slope angle close to 90° due to the existence of "constant phase element" [42]. The straight lines close to 90° indicates a pure capacitive behavior and low diffusion resistance of ions in the structure of the electrodes. The more vertical the curve is, the more closely the supercapacitor behaves as an ideal capacitor. ZnO anchored on the surface of graphene sheets, and the sheets overlapped each other to form a conductive network through sheet plane contact. This structure improves the specific capacitance and preserves the overall high electrical conductivity.

Fig. 8 demonstrates the galvanostatic charge/discharge curves of pure GNS and GNS/ZnO composite electrodes tested from −0.6 to 0.2 V at a constant current density of 10 mA cm^{-2}. All curves exhibit a triangular-shape, implying an ideal capacitor character. In addition, the charge/discharge duration increases in the order of pure GNS < GNS/ZnO (1:3) < GNS/ZnO (1:2) < GNS/ZnO (1:1), indicating the highest specific capacitance for GNS/ZnO (1:1). Fig. 8b shows the charge/discharge curves for the GNS/ZnO (1:1) at the current density of 5 mA cm^{-2}. All curves are linear and symmetrical and no obvious "IR drop" is observed, which means that the electrodes have low internal resistance due to the well-formed electrode/electrolyte interface. The specific capacitances of GNS, GNS/ZnO (1:1), GNS/ZnO (1:2) , GNS/ZnO (1:3) electrodes are 38.6, 62.2, 50.4, and 46.4 F/g, respectively.

Fig. 9 shows the cyclic performances of the electrodes examined by galvanostatic charge/discharge tests for 200 cycles. All electrodes exhibit a little capacitance decay during the tests. For GNS/ZnO (1:1) composite electrode, the capacitance decreases only 5.1% of the initial capacitance after 200 cycles demonstrating an excellent cycle stability and a high degree of reversibility in the repetitive charge/discharge tests.

The maximum power density is also a character of the ESCs, which can be calculated from ESR data [41], according to the

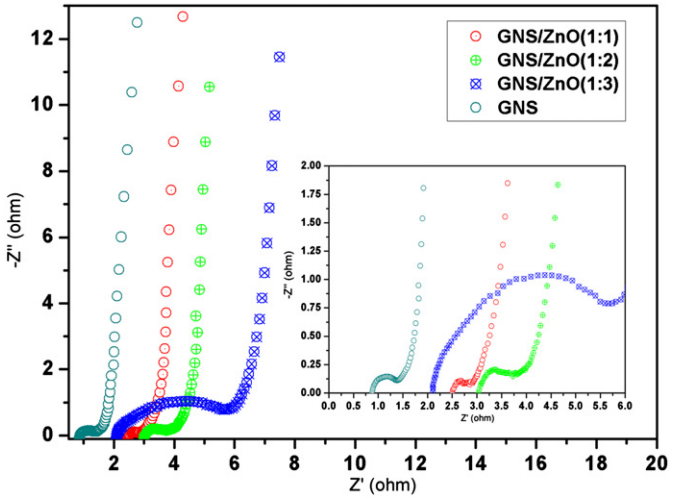

Fig. 7. Nyquist plots of GNS and GNS/ZnO composite electrodes. Inset shows the magnified high-frequency regions.

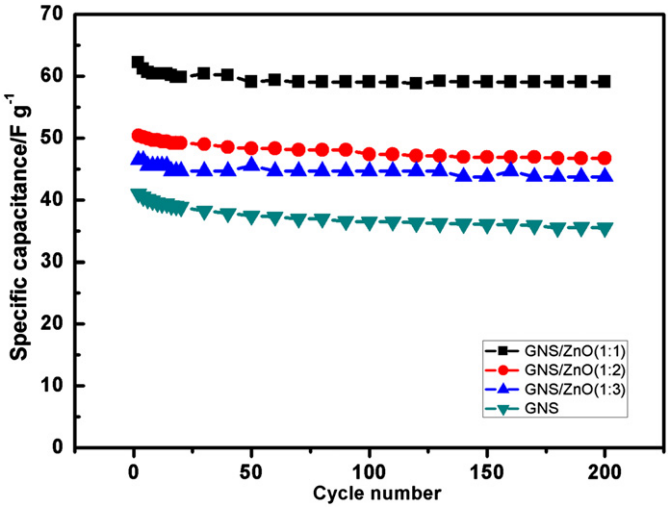

Fig. 9. Cyclic performance of GNS and GNS/ZnO composites electrodes.

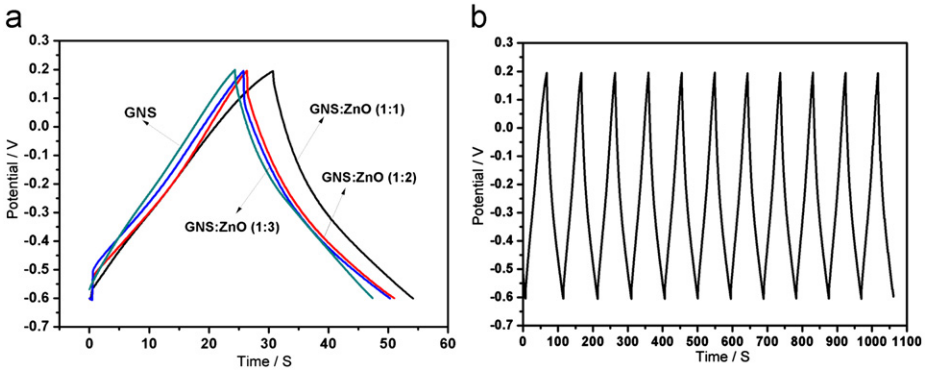

Fig. 8. (a) Galvanostatic charge/discharge profiles of GNS, GNS/ZnO composites with mass ratio of 1:1, 1:2 and 1:3,respectively, and (b) charge/discharge profile for the GNS/ZnO (1:1).

following equation:

$$P_{max} = \frac{V_i^2}{4mR} \quad (2)$$

where V_i is the discharge voltage (V), R is the ESR (Ω), and m is the mass of the electrodes (g). The calculated maximum power density of pure GNS, GNS/ZnO (1:1), GNS/ZnO (1:2), and GNS/ZnO (1:3) is 7.3, 8.1, 4.9 and 3.4 kW/kg, respectively. It further confirmed that the GNS/ZnO composite with the mass ratio of 1:1 has more electrochemical characteristics and is suitable for ESCs compared with other GNS/ZnO composites. The anchored ZnO is the main factor to improve total capacitance for GNS/ZnO composite electrodes. At the same time, the conductivity of the composite is improved by GNS, while more ZnO is not beneficial, implying that a suitable mass ratio is very important for the GNS/ZnO composite electrode.

4. Conclusion

GNS/ZnO composites as electrodes for supercapacitors were prepared by a green synthesis method. The surface morphology, structure and capacitive behaviors of pure GNS and GNS/ZnO composites were investigated. The incorporation of ZnO onto graphene can prevent the agglomeration of graphene sheets and improve the capacitance of composite electrode, the electrolyte/electrode accessibility as well as conductivity. All the synthesized electrode materials show excellent recycling capabilites by galvanostatic charge/discharge tests. GNS/ZnO (1:1) composite electrode exhibits the highest capacitance of 62.2 F/g and power density of 8.1 kW/kg, compared with pure GNS electrode and other types of GNS/ZnO composite electrodes is, therefore, a promising electrode material for ESCs.

Acknowledgments

This work was supported by the Fundamental Research Funds of the Central University (HEUCF101010), Science and Technology Planning Project from Education Department of Heilongjiang Province (11553044), China Postdoctoral Science Foundation (AUGA41309003), Special Innovation Talents of Harbin Science and Technology (2010RFXXG007), the foundation of Harbin Engineering University (HEUFT07053).

References

[1] Y.G. Guo, J.S. Hu, L.J. Wan, Adv. Mater. 20 (2008) 2878–2887.
[2] B.E. Conway, Electrochemical Supercapacitors, Scientific Fundamentals and Technological Applications, Kluwer Academic Publishers, Plenum Press, New York, 1999.
[3] A. Burke, J. Power Sources 91 (2000) 37–50.
[4] R. Kötz, M. Carlen, Electrochim. Acta 45 (2000) 2483–2498.
[5] E. Frackowiak, F. Béguin, Carbon 39 (2001) 937–950.
[6] L. Cao, F. Xu, Y.Y. Liang, H.L. Li, Adv. Mater. 16 (2004) 1853–1857.
[7] H. Wang, H.S. Casalongue, Y. Liang, H. Dai, J. Am. Chem. Soc. 132 (2010) 7472–7477.
[8] G.W. Yang, C.L. Xu, H.L. Li, Chem. Commun. 48 (2008) 6537–6539.
[9] S. Chen, J. Zhu, X. Wang, J. Phys. Chem. C 114 (2010) 11829–11834.
[10] J. Zhang, L.B. Kong, J.J. Cai, H. Li, Y.C. Luo, L. Kang, Microporous Mesoporous Mater. 132 (2010) 154–162.
[11] A. Malak-Polaczyk, C. Matei-Ghimbeu, C. Vix-Guterl, E. Frackowiak, J. Solid State Chem. 183 (2010) 969–974.
[12] Z.A. Hu, Y.L. Xie, Y.X. Wang, L.P. Mo, Y.Y. Yang, Z.Y. Zhang, Mater. Chem. Phys. 114 (2009) 990–995.
[13] K. Wang, J. Huang, Z. Wei, J. Phys. Chem. C 114 (2010) 8062–8679.
[14] Y. Fang, J. Liu, D.J. Yu, J.P. Wicksted, K. Kalkan, C.O. Topal, B.N. Flanders, J. Wu, J. Li, J. Power Sources 195 (2010) 674–1401.
[15] K. Zhang, L.L. Zhang, X.S. Zhao, J. Wu, Chem. Mater. 22 (2010) 1392–1401.
[16] K.S. Novoselov, A.K. Geim, S.V. Morozov, D. Jiang, Y. Zhang, S.V. Dubonos, I.V. Grigorieva, A.A. Firsov, Science 306 (2004) 666–669.
[17] K.S. Novoselov, D. Jiang, F. Schedin, PNAS 102 (2005) 10451–10453.
[18] P.V. Kamat, J. Phys. Chem. Lett. 1 (2009) 520–527.
[19] P.V. Kamat, J. Phys. Chem. Lett. 1 (2010) 587–588.
[20] M.D. Stoller, S. Park, Y. Zhu, J. An, R.S. Ruoff, Nano Lett. 8 (2008) 3498–3502.
[21] S. Vivekchand, C.S. Rout, K. Subrahmanyam, A. Govindaraj, C. Rao, J. Chem. Sci. 120 (2008) 9–13.
[22] H.L. Guo, X.F. Wang, Q.Y. Qian, F.B. Wang, ACS Nano 3 (2009) 2653–2659.
[23] G. Williams, B. Seger, P.V. Kamat, ACS Nano 2 (2008) 1487–1491.
[24] F. Li, J. Song, H. Yang, S. Gan, Q. Zhang, D. Han, A. Ivaska, Nanotechnology 20 (2009) 455602.
[25] M. Law, L.E. Greene, J.C. Johnson, R. Saykally, P.D. Yang, Nat. Mater. 4 (2005) 455–459.
[26] Y. Wang, X. Li, N. Wang, X. Quan, Y. Chen, Sep. Purif. Technol. 62 (2008) 727–732.
[27] C. Tian, W. Li, K. Pan, Q. Zhang, G. Tian, W. Zhou, H. Fu, J. Solid State Chem. 183 (2010) 2720–2725.
[28] Y. Ito, M. Nyce, R. Plivelich, M. Klein, D. Steingart, S. Banerjee, J. Power Sources 196 (2011) 2340–2345.
[29] G. Bronoel, A. Millot, N. Tassin, J. Power Sources 34 (1991) 243–255.
[30] M. Selvakumar, D. Krishna Bhat, A. Manish Aggarwal, S. Prahladh Iyer, G. Sravani, Phys. B: Condens. Matter 405 (2010) 2286–2289.
[31] T. Lu, Y. Zhang, H. Li, L. Pan, Y. Li, Z. Sun, Electrochim. Acta 55 (2010) 4170–4173.
[32] C. Zhu, S. Guo, Y. Fang, S. Dong, ACS Nano 4 (2010) 2429–2437.
[33] W.S. Hummers, R.E. Offeman, J. Am. Chem. Soc. 80 (1958) 1339.
[34] G. Wang, X. Shen, J. Yao, J. Park, Carbon 47 (2009) 2049–2053.
[35] A.C. Ferrari, J. Robertson, Phys. Rev. B 61 (2000) 14095.
[36] C. Gómez-Navarro, R.T. Weitz, A.M. Bittner, M. Scolari, A. Mews, M. Burghard, K. Kern, Nano Lett. 7 (2007) 3499–3503.
[37] S. Stankovich, D.A. Dikin, R.D. Piner, K.A. Kohlhaas, A. Kleinhammes, Y. Jia, Y. Wu, S.T. Nguyen, R.S. Ruoff, Carbon 45 (2007) 1558–1565.
[38] C.J. Youn, T.S. Jeong, M.S. Han, J.H. Kim, J. Cryst. Growth 261 (2004) 526–532.
[39] J.F. Scott, Phys. Rev. B 2 (1970) 1209.
[40] X. Fan, W. Peng, Y. Li, X. Li, S. Wang, G. Zhang, F. Zhang, Adv. Mater. 20 (2008) 4490–4493.
[41] Y. Wang, Z. Shi, Y. Huang, Y. Ma, C. Wang, M. Chen, Y. Chen, J. Phys. Chem. C 113 (2009) 13103–13107.
[42] G.J. Brug, A.V. Eeden, M. Sluyters-Rehbach, J.H. Sluyters, J. Electroanal. Chem. 176 (1984) 275.